A 2000 year rupture history for the Alpine Fault derived from Lake Ellery, South Island New Zealand.

Authors

Jamie D. Howarth[1,2,*], Sean J. Fitzsimons[2], Richard J. Norris[3], Robert Langridge[1] and Marcus J. Vandergoes[1]

[1]*GNS Science, PO Box 30-368, Lower Hutt, New Zealand*

[2]*Department of Geography, University of Otago, PO Box 56, Dunedin, New Zealand*

[3]*Department of Geology, University of Otago, PO Box 56, Dunedin, New Zealand*

***** *Correspondence to: Jamie Howarth*
Address: *Department of Active Landscapes, GNS Science, PO Box 30-368, Lower Hutt, New Zealand*
Ph: *+64 4 570 4228*
Email: j.howarth@gns.cri.nz

Supplementary information:

Suppmentary methods:

Grainsize analysis was conducted on deposits that were traceable across multiple cores from within the lake basin. These deposits were sub-sampled at 10 mm resolution and treated with 5 ml of 30% H_2O_2 at 50 °C for 12 hours and by adding 10 ml of 1 M NaOH to the samples and heating them to 50 °C for 4 hours to remove organic matter and biogenic silica respectively. Samples were then shaken for 30 min, before they were reheated to 50 °C for a further 30 min. The samples were then treated with 5 ml of 5% sodium hexametaphosphate solution and shaken gently for two hours to deflocculate clay-sized particles before analysis. After deflocculation grainsize was analysed on a Malvern Mastersizer 2000G laser diffraction particle size analyser coupled to a HydroG dispersion unit.

Core EL1 was sampled at 10 mm intervals to determine total organic carbon (TOC) and total nitrogen (TN). Individual 10 mm slices of core were sampled from a quarter of the core using a scalpel and 3 mm of material was removed from the margins of each sample to avoid sediment that was in contact with the core liner. Samples were covered in aluminium foil to prevent contamination and then air dried at 36 °C for 48 hours. Dried samples were homogenised using a mortar and pestle and stored in polypropylene test tubes until analysed. The presence or absence of inorganic carbon was determined by treating a subset of samples taken at 100 mm intervals in the cores with 6 N HCL and observing them for an effervescent reaction. None of the samples effervesced so the samples were deemed not to need pre-treatment to remove inorganic carbon and total carbon was regarded as equivalent to TOC. In the absence of carbonates the decision not to pre-treat the samples with acid was conservative considering that recent studies have demonstrated substantial non-linear variation in organic C and N concentrations caused by acid pre-treatment (Brodie *et al.*, 2011; Fernandes and Krull, 2008).

Three hundred milligrams of sample was analysed using a Verio Max elemental analyser running in C/N mode. The Verio Max elemental analyser combusted samples at 900 °C in the presence of an oxygen atmosphere. After combustion carbon and nitrogen compounds were reduced to CO_2 and N_2 using a copper oxide reduction column and the amounts of these gasses counted by a thermal conductivity detector (TCD). Raw counts for C and N were converted to weight percent using a conversion factor derived from glutamic acid standards (N = 9.52±0.05%, C = 40.78±0.2%). Procedural blanks demonstrated that contamination from C and N during the preparation procedure was minimal but present and all sample C and N values were corrected for average procedural blanks (n = 20). The precision of results was assessed by measuring duplicate samples every 200 mm down core EL1 and is reported as the average difference between replicates, which is ±0.001%

The core density and TOC data were used to calculate mass of clastic sediment (M_{cs}) in core EL1 using the methods outlined in Howarth et al. (2012). The mass of clastic sediment (M_{cs}) in 10 mm sections of core EL1 was determined by multiplying core volume by the dry density of clastic sediment. The dry density of clastic sediment was calculated using equation S1:

$$Mcs = \left(\frac{M_{wet}}{\left(1 + \frac{W}{100}\right)} \right) - \left(\left(\frac{M_{wet}}{\left(1 + \frac{W}{100}\right)} \right) \times \left(\frac{F(TOC)}{100} \right) \right) \quad \text{(S1)}$$

where M_{wet} is the wet mass of the sediment in a 1 cm slice of core (g), W is weight percentage water content (%), TOC is total organic carbon (%) and F is the Van Bemmelen factor of 1.724 for converting weight percent TOC to weight percent organic matter.

References:

Berryman, K., Cooper, A., Norris, R., Villamor, P., Sutherland, R., Wright, T., Schermer, E., Langridge, R., and Biasi, G., 2012b, Late Holocene rupture history of the Alpine Fault in South Westland, New Zealand. Bulletin of the Seismological Society of America, v. 102, p. 620-638.

Brodie, C. R., Leng, M. J., Casford, J. S. L., Kendrick, C. P., Lloyd, J. M., Yongqiang, Z. and Bird, M. I., 2011, Evidence for bias in C and N concentrations and δ13C composition of terrestrial and aquatic organic materials due to pre-analysis acid preparation methods. Chemical Geology, v. 282, p. 67-83.

Bronk Ramsey, C., and Lee, S., 2013, Recent and Planned Developments of the Program OxCal. Radiocarbon, v. 55, p. 720-730.

Fernandes, M. and Krull, E., 2008, How does acid treatment to remove carbonates affect the isotopic and elemental composition of soils and sediments? Environmental Chemistry, v. 5, p. 33-39.

Howarth, J. D., Fitzsimons, S. J., Norris, R. J., and Jacobsen, G. E., 2012, Lake sediments record cycles of sediment driven by large earthquakes on the Alpine Fault, New Zealand. Geology, v. 40, p. 1091-1094.

Howarth, J. D., Fitzsimons, S. J., Norris, R. J., and Jacobsen, G. E. 2014, Lake Sediments record high intensity shaking that provides insight into the location and rupture length of large earthquakes on the Alpine Fault, New Zealand. Earth and Planetary Science Letters, v. 403, 340-351.

Supplementary note: OxCal 4.2 code for the revised Haast, Okuru and Turnbull trench chronology. In this prior model each trench is represented individually but the event horizons (EH) are tied.

```
Options()
{
 Curve="ShCal13.14c";
};
Plot()
{
 Sequence("Haast_South")
 {
  Boundary("Base of  section");
  Date("=EH3");
  R_Date("5p", 900, 57);
  Date("=EH2");
  R_Date("4i", 625, 57);
  Date("=EH1");
  C_Date("Historic period", 1840, 2);
  Boundary("Top of sections");
 };
 Sequence("Okuru_North")
 {
  Boundary("Base of  section");
  Date("EH3");
  Phase("5p")
  {
   R_Date("5p", 790, 60);
   R_Date("5p", 400, 120);
  };
  Date("EH2");
  R_Date("4w", 520, 160);
  Date("EH1");
  R_Date("3w", 258, 56);
  C_Date("Historic period", 1840, 2);
  Boundary("Top of sections");
 };
 Sequence("Okuru_South")
 {
  Boundary("Base of  section");
  Date("=EH2");
  R_Date("4i", 660, 60);
  Date("=EH1");
  C_Date("Historic period", 1840, 2);
  Boundary("Top of sections");
 };
 Sequence("Turnbull")
 {
  Boundary("Base of  section");
  Phase("6p")
  {
   R_Date("Wk8122", 1410, 50);
   R_Date("Wk8301", 1390, 60);
   R_Date("Wk8123", 1000, 50);
  };
  Date("=EH3");
  Phase("5p")
  {
   R_Date("11498", 1083, 60);
  };
  Date("=EH2");
  C_Date("Historic period", 1840, 2);
  Boundary("Top of sections");
 };
};
```

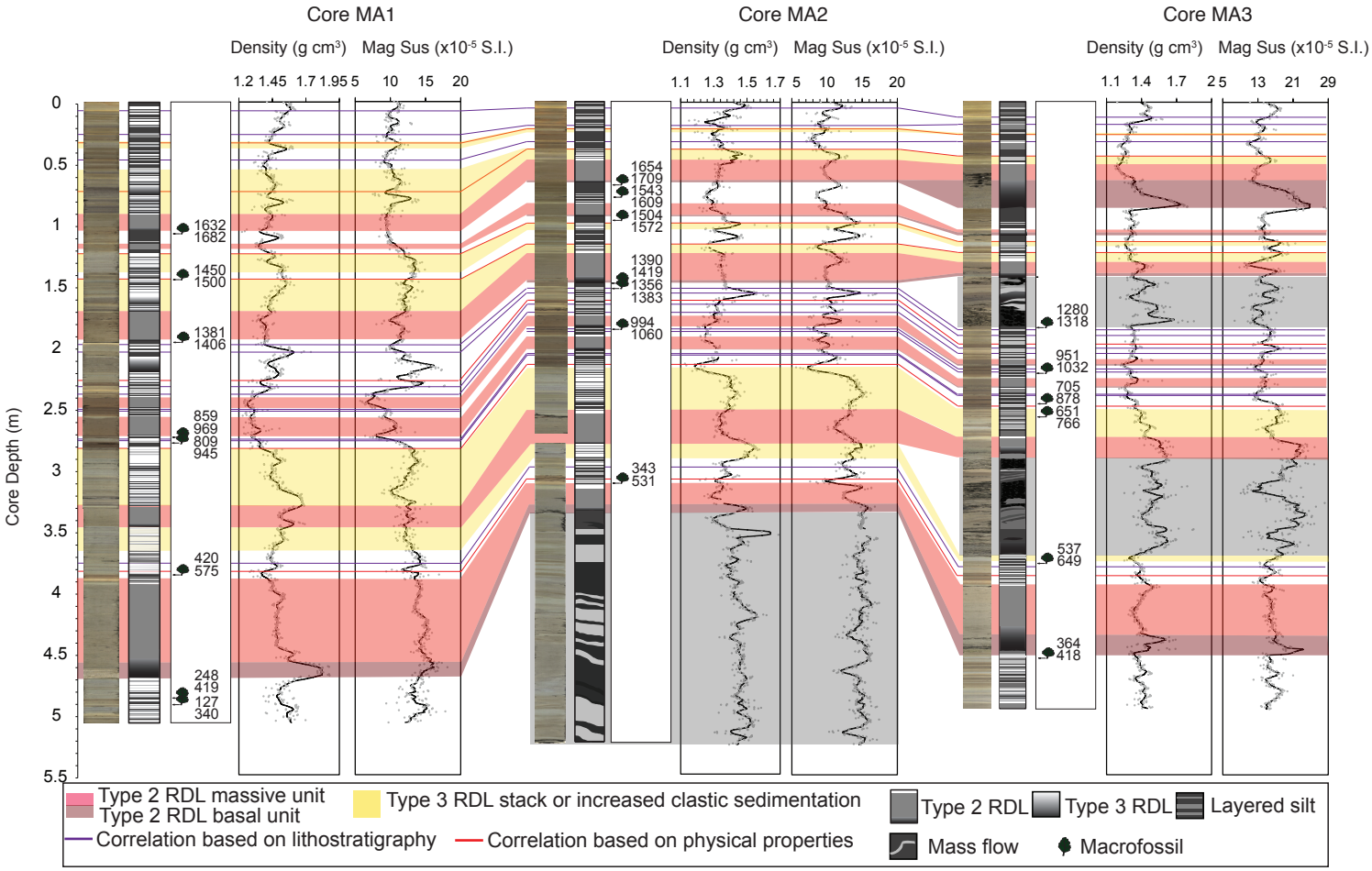

Figure S1: Summary of the sedimentary record from Lake Mapourika extended from that presented by Howarth et al. (2014), containing digital images, graphic logs, terrestrial macrofossil 95% highest probability density age ranges, gamma density and magnetic susceptibility for cores MA1 (left) from the southern sub-basin and, cores MA2 (centre) and MA3 (right) from the northern sub-basin of Lake Mapourika. Dark red and red shading shows the geometry of the thinning basinward basal units and the basinward thickening homogenous units of type 2 RDLs, respectively. These units can be correlated across the basin. Yellow shading shows type 3 RDL stacks and increases in clastic sedimentation that correlate across the sub-basins. Purple and red horizontal lines represent core to core correlations based on lithostratigraphy and physical properties, respectively.

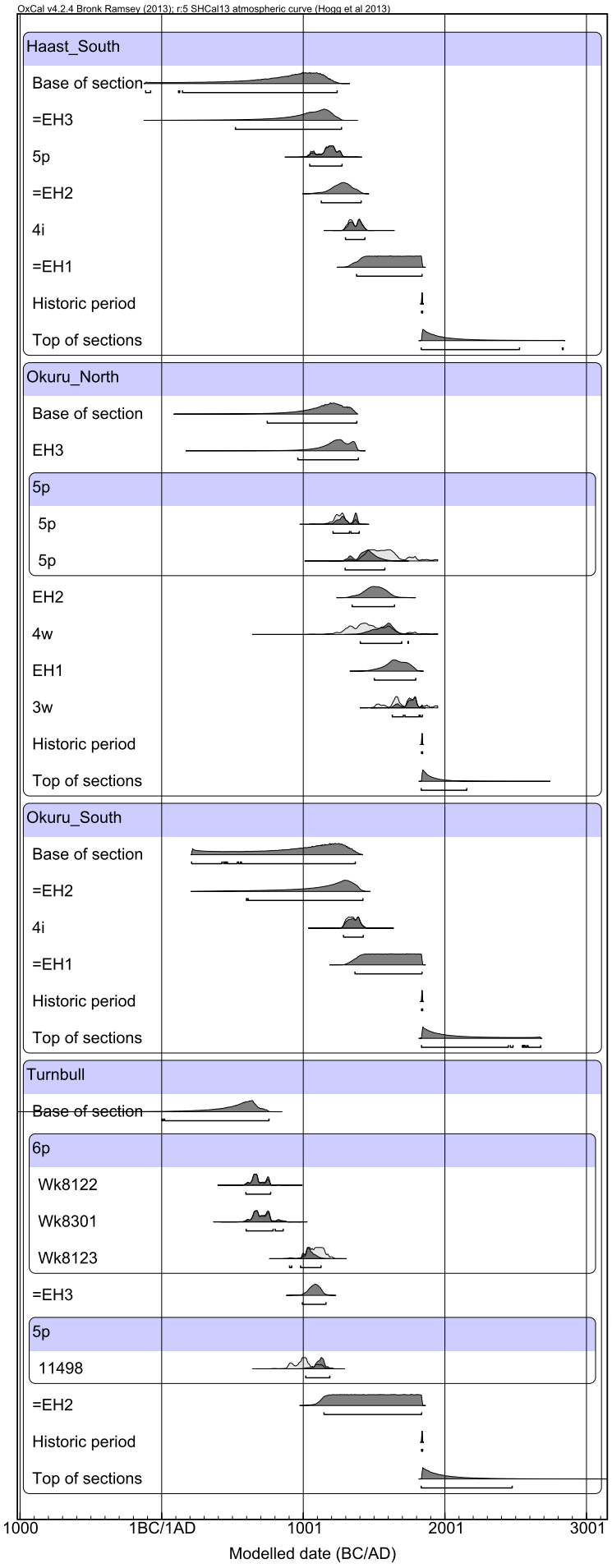

Figure S2: Revised age model for the Haast trench sites produced in OxCal 4.2 (Bronk Ramsey and Lee, 2013).

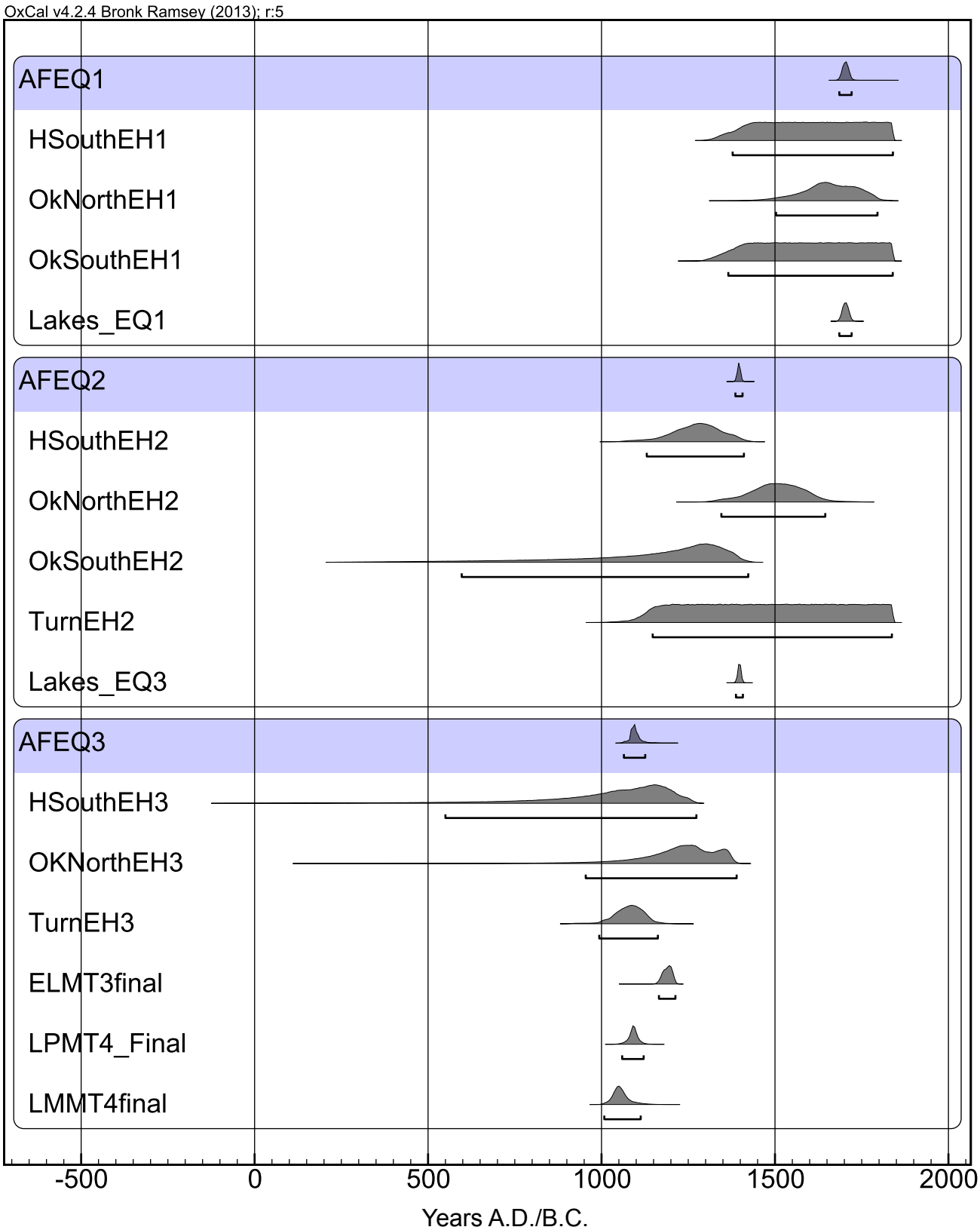

Figure S3: Comparison of event sequence age PDFs for the last three earthquakes from the Haast, Okuru and Turnbull trenches as well as the lake Ellery, Paringa and Mapourika records (Berryman et al., 2012b; this study). Bars represent the 95% highest probability density function range. AFEQ – Alpine Fault earthquakes; EH – event sequence; Hsouth - Haast River South Trench; OkNorth – Okuru River North Trench; OkSouth – Okuru River South Trench; and Turn – Turnbull River Trench.

Table S1: Summary information for conventional radiocarbon ages (CRAs) from Lake Ellery.

Lab code	RDL* normalised depth (cm)	Macrofossil type	$\delta^{13}C$ (‰)	^{14}C age (yr BP)	95% modelled age HPDF (A.D.)
NZA 51739	19.5	Unknown leaf	-27.2±0.2	138±20	1950-1696
NZA 51877	21.4	Unknown seed	-26.2±0.2	166±20	1950-1675
NZA 51737	43.8	W. racemosa leaf	-24.8±0.2	229±20	1802-1654
NZA 51783	46.0	Unknown leaf	-28.4±0.2	353±21	1641-1499
NZA 51803	54	N. menzesii leaf	-29.9±0.2	351±20	1641-1498
NZA 51804	58.5	N. menzesii leaf	-30.0±0.2	437±20	1613-1447
NZA 51805	60.8	W. racemosa leaf	-27.6±0.2	449±20	1610-1442
NZA 51806	68.1	N. menzesii leaf	-29.6±0.2	699±24	1416-1320
NZA51866	74.3	D. cupressinum leaf	-29.4±0.2	613±20	1391-1286
NZA 51874	80.8	N. menzesii leaf	-31.1±0.2	776±20	1297-1229
NZA 51876	84.3	W. racemosa leaf	-29.0±0.2	844±20	1275-1209
NZA 51910	88.9	N. menzesii leaf	-28.8±0.2	931±19	1218-1053
NZA 51829	92.9	N. menzesii leaf	-29.3±0.2	922±20	1214-1050
NZA 38101	96	N. menzesii leaf	-30.4±0.2	988±24	1154-1030
NZA 38106	101.2	N. menzesii leaf	-28.4±0.2	1029±25	1149-996
NZA 38100	107.4	N. menzesii leaf	-28.5±0.2	1037±25	1145-993
NZA 38099	110.5	N. menzesii leaf	-32.2±0.2	1059±25	1134-987
NZA 51830	114.1	N. menzesii leaf	-30.0±0.2	1125±20	1019-895
NZA 38104	118.1	N. menzesii leaf	-27.7±0.2	1140±25	1013-890
NZA 38105	120.6	N. menzesii leaf	-31.0±0.2	1175±25	986-883
NZA 51807	124.3	N. menzesii leaf and a N. solandri leaf	-31.9±0.2	1269±21	884-691
NZA 38102	129.4	N. menzesii leaf	-28.4±0.2	1352±25	855-673
NZA 38103	131.2	N. menzesii leaf	-27.7±0.2	1319±25	768-663
NZA 51831	138.8	N. solandri leaf	-27.9±0.2	1481±20	650-588
NZA 51869	146.8	N. menzesii leaf	-29.8±0.2	1523±21	638-545
NZA 51896	150.5	N. solandri leaf	-29.6±0.2	1630±20	577-437
NZA 51895	153.3	N. menzesii leaf	-30.4±0.2	1590±20	531-417
NZA 51902	162.6	W. racemosa leaf	-31.1±0.2	1689±20	464-357
NZA 51894	173.4	N. menzesii leaf	-32.1±0.2	1714±20	420-258
NZA 51911	178.7	N. menzesii leaf	-30.0±0.2	1801±20	355-225
NZA 51898	184.0	N. solandri leaf	-27.8±0.2	1825±20	340-144
NZA 51906	191.1	N. menzesii leaf	-28.6±0.2	1937±20	226-114
NZA 51905	192.6	N. menzesii leaf	-28.8±0.2	1896±20	200-59
NZA 51904	196.9	N. menzesii leaf	-30.4±0.2	1982±20	118--37
NZA 51901	202.3	N. menzesii leaf	-29.9±0.2	2098±20	17--140
NZA 51899	208.8	N. menzesii leaf	-27.3±0.2	2160±20	-66--341

*Core depth with rapidly deposited layers removed.

Table S2: Timing of subaqueous mass-wasting events in lakes Ellery, Paringa and Mapourika, durations of increased postseismic terrestrial sediment flux and mass accumulation rates.

Event timing (A.D./B.C.)	Timing of Event Sequence (A.D./B.C.)			χ^2 Test P value	Duration of post-seismic sediment flux (yr)			Lake Ellery MAR (g cm^{-1} yr^{-2})	
	Ellery	Paringa	Mapourika		Ellery	Paringa	Mapourika	Postseismic	Interseismic
1726-1690	1770-1680	1744-1690* 1745-1690†	1791-1657* 1734-1658‡	<0.05	32±17	78±14	N/D	0.18±0.13	0.07±0.02
1407 -1388	1428-1362	1408-1372* 1405-1374†	1420-1388* 1422-1390‡	<0.05	60±18	39±8	50±12	0.09±0.05	0.05±0.01
1213-1008	1213-1165	1122-1059* 1120-1064†	1113-1008* 1090-1015‡	>0.05	23±14	72±12	N/D	0.13±0.10	0.08±0.03
1008 - 966	1024-967	1010-945* N/D	N/A N/A	<0.05	19±12	N/A	N/D	0.2±0.16	0.08±0.02
961 - 915	991-915	966-883* 965-887†	974-845* 977-869‡	<0.05	22±15	51±11	N/D	0.13±0.11	0.04±0.03
646 - 592	645-584	N/A N/A	671-571* N/D	<0.05	29±17	N/A	N/D	0.13±0.10	0.04±0.01
416 - 370	430-329	N/A N/A	420-364* N/D	<0.05	22±14	N/A	N/D	0.64±0.51	0.04±0.01
206 - 93	206-93	N/A	N/A	N/A	24±18	N/A	N/A	0.15±0.13	0.7±0.03
20 - 150	150-20	N/A	N/A	N/A	16±15	N/A	N/A	0.14±0.14	0.04±0.02
Averages					27±5	58±7		0.19±0.07	0.06±0.01

Notes:
Event sequence ages reported as 95% highest probability density function; Errors on durations and rates are reported to 1 standard error; N/A – not applicable; N/D – no data; MAR – mass accumulation rate
* ages determined from the P_sequence age model with variable constant k
†ages from Howarth et al. (2012).
‡ages from Howarth et al. (2014).